Ocean Dynamics (2017) 67:345–356
DOI 10.1007/s10236-017-1031-x

Mesoscale circulation along the Sakhalin Island eastern coast

Sergey V. Prants[1] · **Andrey G. Andreev**[1] · **Michael Yu. Uleysky**[1] · **Maxim V. Budyansky**[1]

Received: 10 August 2016 / Accepted: 15 January 2017 / Published online: 2 February 2017

Abstract The seasonal and interannual variability of mesoscale circulation along the eastern coast of the Sakhalin Island in the Okhotsk Sea is investigated using the AVISO velocity field and oceanographic data for the period from 1993 to 2016. It is found that mesoscale cyclones with the horizontal dimension of about 100 km occur there predominantly during summer, whereas anticyclones occur predominantly during fall and winter. The cyclones are generated due to a coastal upwelling forced by northward winds and the positive wind stress curl along the Sakhalin coast. The anticyclones are formed due to an inflow of low-salinity Amur River waters from the Sakhalin Gulf intensified by southward winds and the negative wind stress curl in the cold season. The mesoscale cyclones support the high biological productivity at the eastern Sakhalin shelf in July – August.

Keywords Okhotsk Sea · East Sakhalin current · Mesoscale circulation cells · Seasonal variability

1 Introduction

The Okhotsk Sea (OS) is one of the marginal seas in the North Pacific. It is bounded by the Kamchatka Peninsula, Siberia, Sakhalin Island (SI), Hokkaido, and the Kuril Islands. The OS is connected to the subarctic North Pacific through the Kuril Islands chain. About 50–70 % of the OS area is covered with ice in winter. The distribution of dynamic topography in the OS indicates a general cyclonic circulation in the north and an anticyclonic circulation in the deep Kuril Basin in the south (Moroshkin 1966; Ohshima et al. 2004). The East Sakhalin Current (ESC) is the western boundary current of the OS cyclonic gyre (Fig. 1). The ESC transports southward low salinity surface water, affected by the Amur River discharge, along the eastern SI shelf-break.

The intensity and direction of the ESC change seasonally. The seasonal maps of the geostrophic currents (relative to 500 dbar with the data collected between 1948 and 1994) demonstrate a strong southward flux along the eastern SI shelf and slope in late fall and a weak northward flux along 200 m isobath in summer (Pishchalnik and Arhipkin 1999). The northward flow in the surface layer along the northeastern Sakhalin shelf (52.5° N) during August and first decade of September and the strong southward flow during the second and third decades of September 1997 and 1998 have been observed by Kochergin et al. (1999). They indicated a positive correlation between meridional wind and meridional velocity (mooring data). Ohshima et al. (2004) have demonstrated by using the wind stress curl and mooring data that the computed Sverdrup transport and the observed ESC transport (53° N, July 1998 – January 2000, depth ∼100 m) exhibit large seasonal variations with maximum in winter and minimum in summer. They assumed that the main part (the shelf-slope core) of the ESC can be regarded as a western boundary current of the wind-driven cyclonic gyre. The lack of the observed northward transport of the ESC across 53° N in summer of 1999 during the period of the negative (anticyclonic) wind stress curl was explained by the importance of the annually mean wind stress curl for the southward flow of the ESC in summer. Ebuchi (2006) has studied the seasonal and interannual variations in the ESC

Responsible Editor: Alejandro Orfila

✉ Sergey V. Prants
prants@poi.dvo.ru

[1] Pacific Oceanological Institute of the Russian Academy of Sciences, Vladivostok, Russia

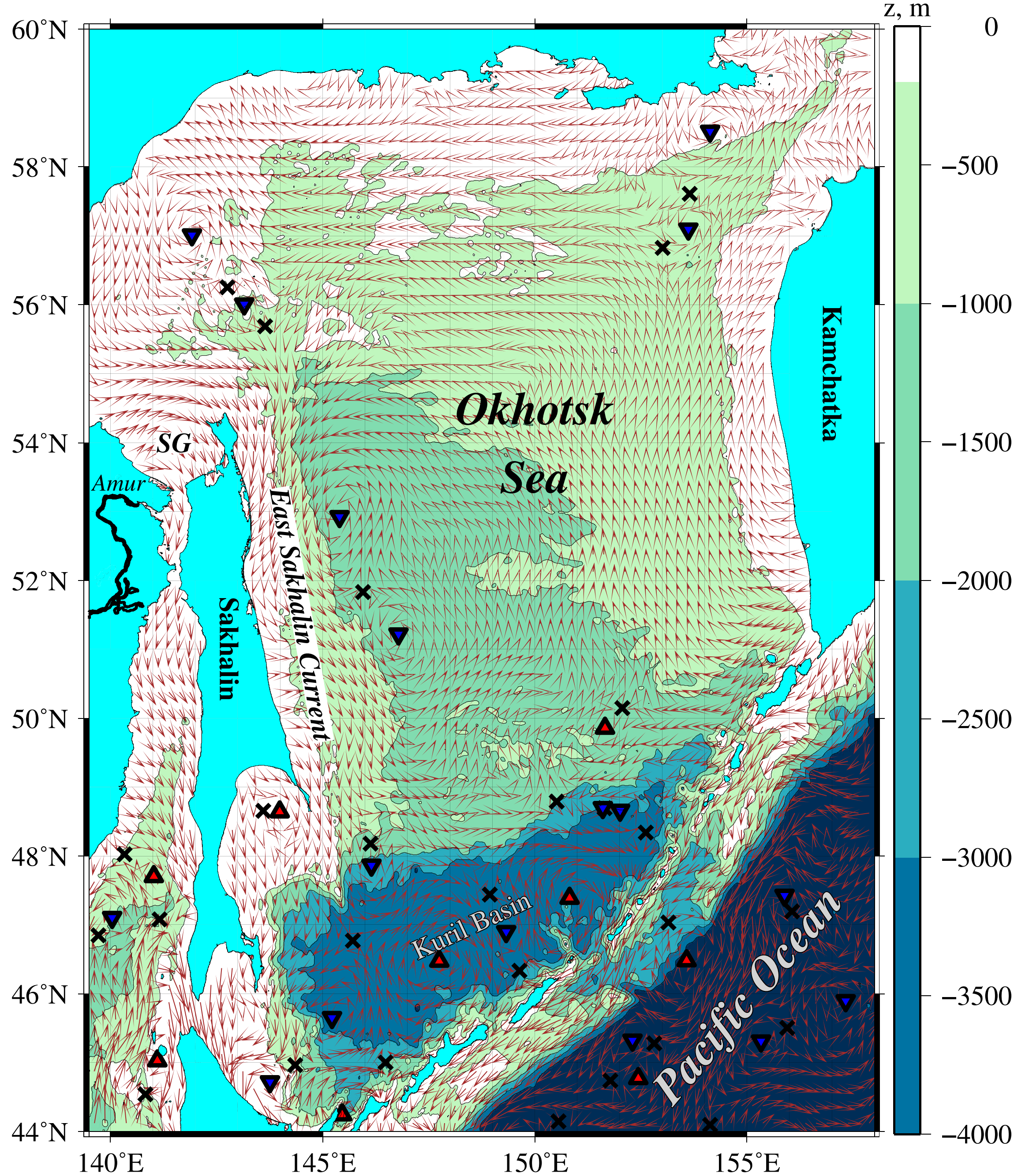

Fig. 1 The bathymetry of the Okhotsk Sea with the altimetric AVISO velocity field imposed (*the arrows*) averaged for the period from 1993 to 2016. The elliptic and hyperbolic stagnation points with zero mean velocity are indicated by the *triangles* and *crosses*, respectively. SG is for the Sakhalin Gulf

and its relation to wind stress and wind stress curl fields in the OS using ten-year (1992–2002) records of the sea level anomaly observed by the TOPEX/POSEIDON altimeter. He concluded that the southward flow of the ESC is strong in winter and almost disappears in summer and that more observations are required to clarify the relationship between the interannual variations in the ESC and those of the wind fields over the OS.

Using the CTD data collected in summer 1994, Verkhunov (1997) revealed the mesoscale cyclonic circulation off the northeastern SI and the northward transport of the ESC along the slope and the southward transport along the shelf. The existence of the northeastward and northwestward currents along the East Sakhalin slope (51.5° N) in summer 2009 and 2010 has been shown by Kusailo et al. (2013) using the mooring data.

The northeastern SI shelf is known as a region with remarkably high primary production of 1.5–2 g C m^{-2} day^{-1} in the post-spring bloom period (July – August) (Sorokin and Sorokin 2002). The physical processes at the northeastern SI shelf are of a special interest in view of the high productivity of benthos communities eaten here by gray whales during the annual summer-autumn fattening (Meier et al. 2007). The benthos fauna growth is due to a detritus flux provided by the phytoplankton bloom. The mesoscale anticyclones and cyclones, observed off the eastern SI, could have a profound effect on the physical and biological environments and can impact the marine ecosystem at the SI shelf from plankton distribution to higher trophic levels such as feeding and growth of eggs and larvae and benthos.

In this study, we show that the mesoscale cyclones with the horizontal dimension of 100 km occur in the ESC region predominantly during summer, whereas anticyclones are generated predominantly during fall and ice-free winter months (October – December). The mesoscale cyclones generation is related to the coastal upwelling forcing by northward winds and positive wind stress curl along the SI coast. The anticyclones formation is related to inflow of low salinity waters from the Sakhalin Gulf driven by southward winds and the negative wind stress curl along the SI coast.

2 Data and methods

We used the daily geostrophic velocities for the period from January 2, 1993 to March 17, 2016 obtained from the AVISO database on a 1/4° × 1/4° Mercator grid (http://www.aviso.altimetry.fr). The AVISO database combines altimetric data from the TOPEX/POSEIDON mission, from Jason-1 for the data after December, 2001, and from Envisat for the data after March, 2002. Because of a sea ice coverage in the western OS from January to April (Minervin et al. 2015), the altimetry data collected during this period were excluded from the results and discussion. The oceanographic and daily wind data were provided by the World Ocean Database (WOD13) (https://www.nodc.noaa.gov/OC5/WOD), Pacific Oceanological Institute database (http://oias.poi.dvo.ru), and NCEP reanalysis (http://www.esrl.noaa.gov). In our study, we used the scatterometer-derived wind vectors and wind stress curl data (ftp://numbat.coas.oregonstate.edu/pub/scow) (Risien and Chelton 2008) and MODIS SST satellite imagery (http://oceandata.sci.gsfc.nasa.gov).

All the Lagrangian simulation results have been obtained by solving advection equations for a large number of synthetic particles (tracers) advected by the AVISO velocity field

$$\frac{d\lambda}{dt} = u(\lambda, \varphi, t), \qquad \frac{d\varphi}{dt} = v(\lambda, \varphi, t), \tag{1}$$

where u and v are angular zonal and meridional velocities, φ and λ are latitude and longitude, respectively. Bicubical spatial interpolation and third order Lagrangian polynomials in time are used to provide numerical results. Lagrangian trajectories are computed by integrating the Eq. (1) with a fourth-order Runge-Kutta scheme.

In order to track the origin of waters along the eastern SI coast in the warm and cold seasons, we have computed the so-called Lagrangian drift maps with boundaries (Prants 2013; Prants et al. 2013a, 2014, 2015). A domain in the Sea is seeded at a fixed date with a large number of tracers whose trajectories are computed backward in time for a given period of time (Prants 2015). The waters, that entered a given area for that period through different geographical boundaries, are shown by different colors on such a map.

The Lagrangian approach, in particular, seems to be more appropriate to identify eddies and document their modification and interaction with ambient waters than the commonly used techniques, because the Lagrangian maps are imprints of history of water masses involved in the vortex motion whereas vorticity, the Okubo-Weiss parameter and similar indicators are "instantaneous" Eulerian snapshots. So, one can identify eddies and document their transformations more accurately with Lagrangian maps.

For computation of the meridional volume transport of the ESC, M_y, the Sverdrup relation is applied

$$M_y = \int \beta^{-1} \rho^{-1} \operatorname{curl}_z \tau dx, \tag{2}$$

where the vertical component of the wind stress curl equals to $\operatorname{curl}_z \tau = \partial\tau_y/\partial x - \partial\tau_x \partial y$, ρ is the density of water, and β is the meridional derivative of the Coriolis parameter. The integration path is taken along the latitudinal lines from the eastern, 154° E, to western, 144° E, boundaries of the OS. We used the meridional, τ_y, and zonal, τ_x, monthly averaged wind stress data from the NCEP reanalysis.

3 Results

In July – August and November – December, the surface circulation along the eastern SI coast is determined by the mesoscale cyclones and anticyclones, respectively, located off the Piltun Bay and eastward of the Terpeniya Bay (Fig. 2). We call them as the Piltun and Terpeniya circulation cells which are clearly visible in Fig. 2 in the altimetric AVISO velocity field averaged for July – August (Fig. 2a) and November – December (Fig. 2b) from 1993 to 2016. In the warm period, both the cells have a cyclonic circulation (Fig. 2a), whereas in the cold period, they are anticyclones with the diameter of 100 km (Fig. 2b).

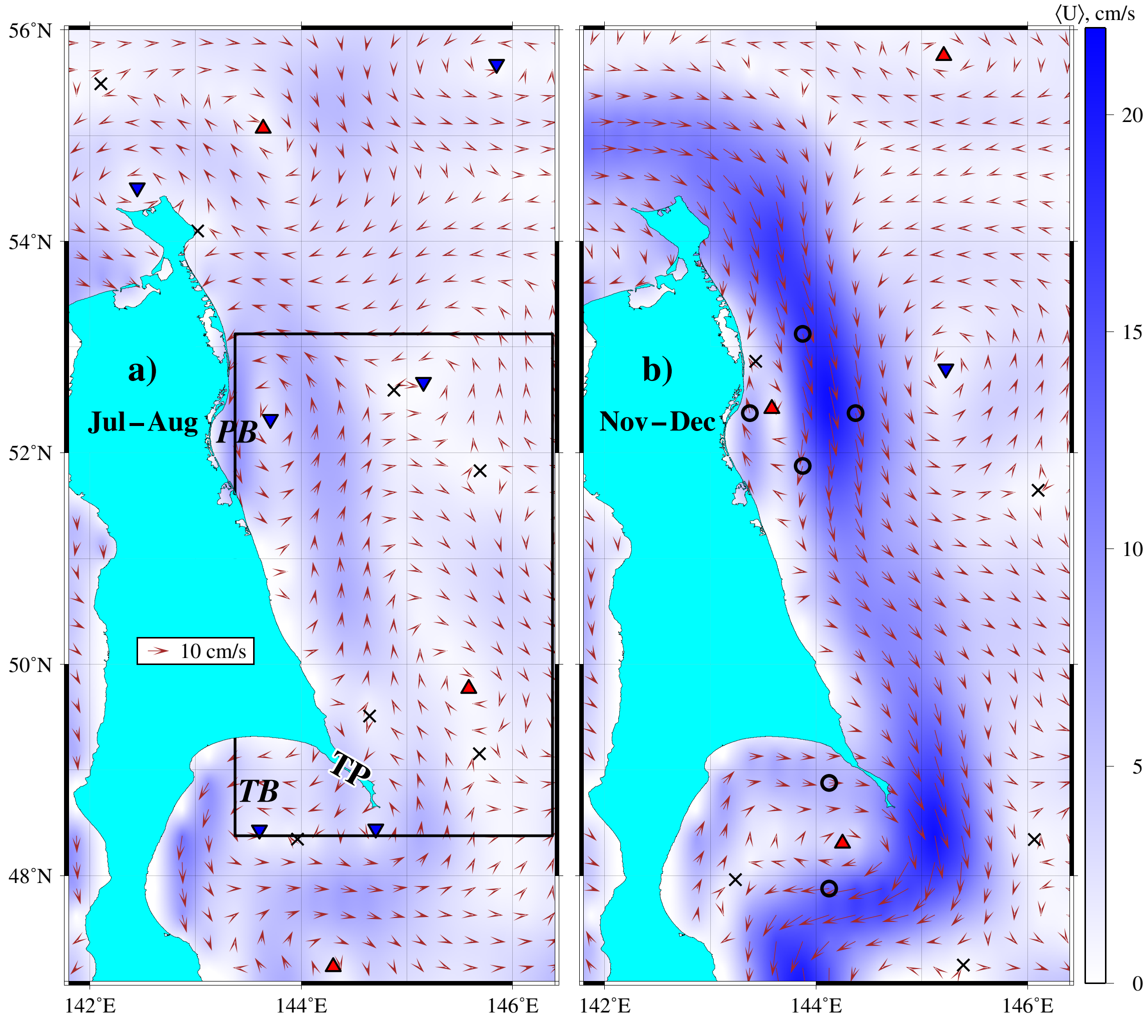

Fig. 2 The altimetric AVISO velocity field around the eastern coast of the Sakhalin Island averaged for **a** July – August and **b** November – December from 1993 to 2016. The magnitudes of the averaged velocity, $\langle U \rangle$, are coded by nuances of the color. The centers of mesoscale cyclones and anticyclones are shown by the *triangles* with downward and upward orientation of one of the triangle's top, respectively. The *hollow circles* represent the circulation cell boundaries. PB and TB stand for the Piltun Bay and Terpeniya Bay, respectively. TP is for the Terpeniya Peninsula

It is useful to compute locations in the AVISO field where the velocity is zero. The standard stability analysis allows to specify stagnation elliptic and hyperbolic points the motion around which is stable and unstable, respectively. The elliptic points are situated mainly at the centers of eddies. The motion around them is stable and circular. The hyperbolic points, situated mainly between and around eddies, are unstable ones with the directions along which fluid particles converge to such a point and another directions along which they diverge. We mark the elliptic points on the Lagrangian maps by triangles and the hyperbolic ones — by crosses. Up (down)ward orientation of one of the triangle's top marks anticyclonic (cyclonic) rotation of water around them. The triangles are colored in the online version as red (blue) ones marking the centers of anticyclones (cyclones). The stagnation points are moving Eulerian features and may undergo bifurcations in the course of time. In spite of nonstationarity of the velocity field, some of them may exist for weeks and much more (Prants 2014, 2015).

The AVISO velocity field, shown in Fig. 2, was averaged for the warm (Fig. 2a) and cold months (Fig. 2b) for the last 23 years. So, the triangles in Fig. 2a with the coordinates (52.3° N, 143.6° E) and (48.4° N, 143.6° E) specify average positions of the centers of the Piltun and Terpeniya cyclonic circulation cells, respectively, which regularly appear there in warm seasons. The triangles in Fig. 2b with the coordinates (52.4° N, 143.5° E) and (48.3° N, 144.2° E) specify average positions of the centers of the Piltun and Terpeniya anticyclonic circulation cells, respectively, which regularly appear there in cold seasons.

In order to illustrate seasonal variations in meridional and zonal AVISO velocities at the boundaries of the Piltun and Terpeniya circulation cells, we plot their variations in Fig. 3 for the period from 2009 to 2016. In Fig. 3a, the temporal changes in the meridional velocities are shown at the western (52.375° N, 143.375° E) and eastern (52.375° N, 144.375° E) boundaries of the Piltun circulation cell. In Fig. 3b, we show the temporal changes in the zonal velocities at the northern (53.125° N, 143.875° E) and southern (51.875° N, 143.875° E) boundaries of the Piltun circulation cell. The temporal changes in the zonal velocities at the northern (48.875° N, 144.125° E) and southern (47.875° N, 144.125° E) boundaries of the Terpeniya circulation cell are shown in Fig. 3c. The surface velocities are equal to 0.1–0.2 (0.2–0.3) m/s (Figs. 3a, b) at the boundaries of the cyclones (anticyclones). In July – August (November – December), the surface flow of the ESC is directed northward (southward) along the SI slope.

The meridional velocities at the western and eastern boundaries (Fig. 3a) and zonal velocities at the northern and southern boundaries (Fig. 3b, c) of the mesoscale circulation cells off the northeastern and southeastern SI undergo significant seasonal variations with positive (negative) values in May – September and negative (positive) values in October – December. The correlation coefficient between the meridional velocities at the eastern and western boundaries of the mesoscale Piltun circulation cell is −0.91 (2009–2016). The correlation coefficients between the meridional velocities at the eastern boundary and the zonal velocities at the northern (southern) boundaries are −0.60 and 0.74.

The seasonal changes of the flow direction at the boundaries of the mesoscale circulation cells demonstrate that the mesoscale cyclones are formed in the eastern SI coast area predominantly during summer, whereas anticyclones are generated predominantly during fall and winter.

The comparison of the geostrophic currents (5/1000 dbar, July 1994) off the eastern SI, computed with the help of the detailed CTD survey data (Verkhunov 1997), with the altimetric AVISO velocity distributions (July 16, 1994) demonstrates a good agreement. Both the velocity fields show the existence of the mesoscale cyclones off the northeastern and southeastern SI (∼49° N and ∼52° N) and mesoscale anticyclone off the northeastern SI (∼55° N).

The oceanographic surveys across the Piltun circulation cell have been carried out in July 2006 and November 1994 when it was cyclonic (Fig. 4a) and anticyclonic (Fig. 4b),

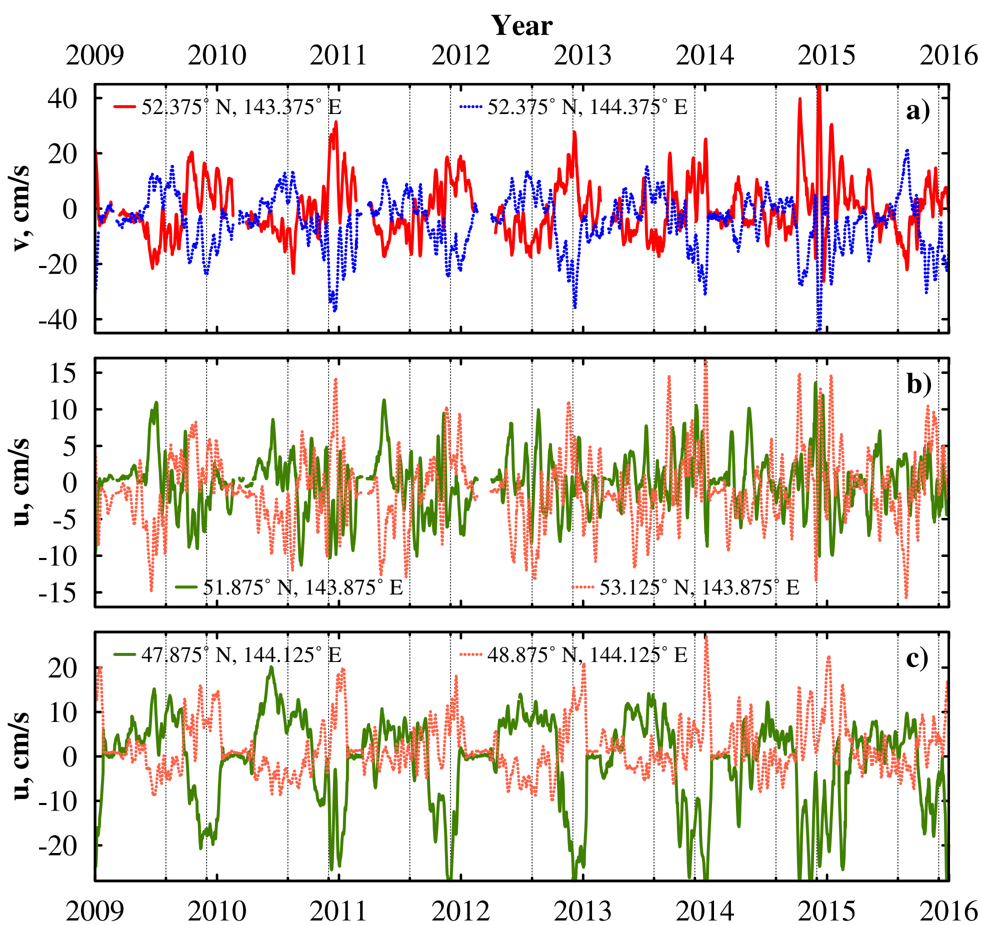

Fig. 3 **a** The temporal changes in the meridional velocities at the western (52.375° N, 143.375° E, the *bold curve*) and eastern (52.375° N, 144.375° E, the *dashed curve*) boundaries of the Piltun circulation cell. **b** The temporal changes in the zonal velocities at the northern (53.125° N, 143.875° E, the *dashed curve*) and southern (51.875° N, 143.875° E, the *bold curve*) boundaries of the Piltun circulation cell. **c** The temporal changes in the zonal velocities at the northern (48.875° N, 144.125° E, the *dashed curve*) and southern (47.875° N, 144.125° E, the *bold curve*) boundaries of the Terpeniya circulation cell. The locations, corresponding to the circulations cell boundaries, are shown by the *hollow circles* in Fig. 2b. The *vertical straight lines* mark August, 1 and December, 1 for each year

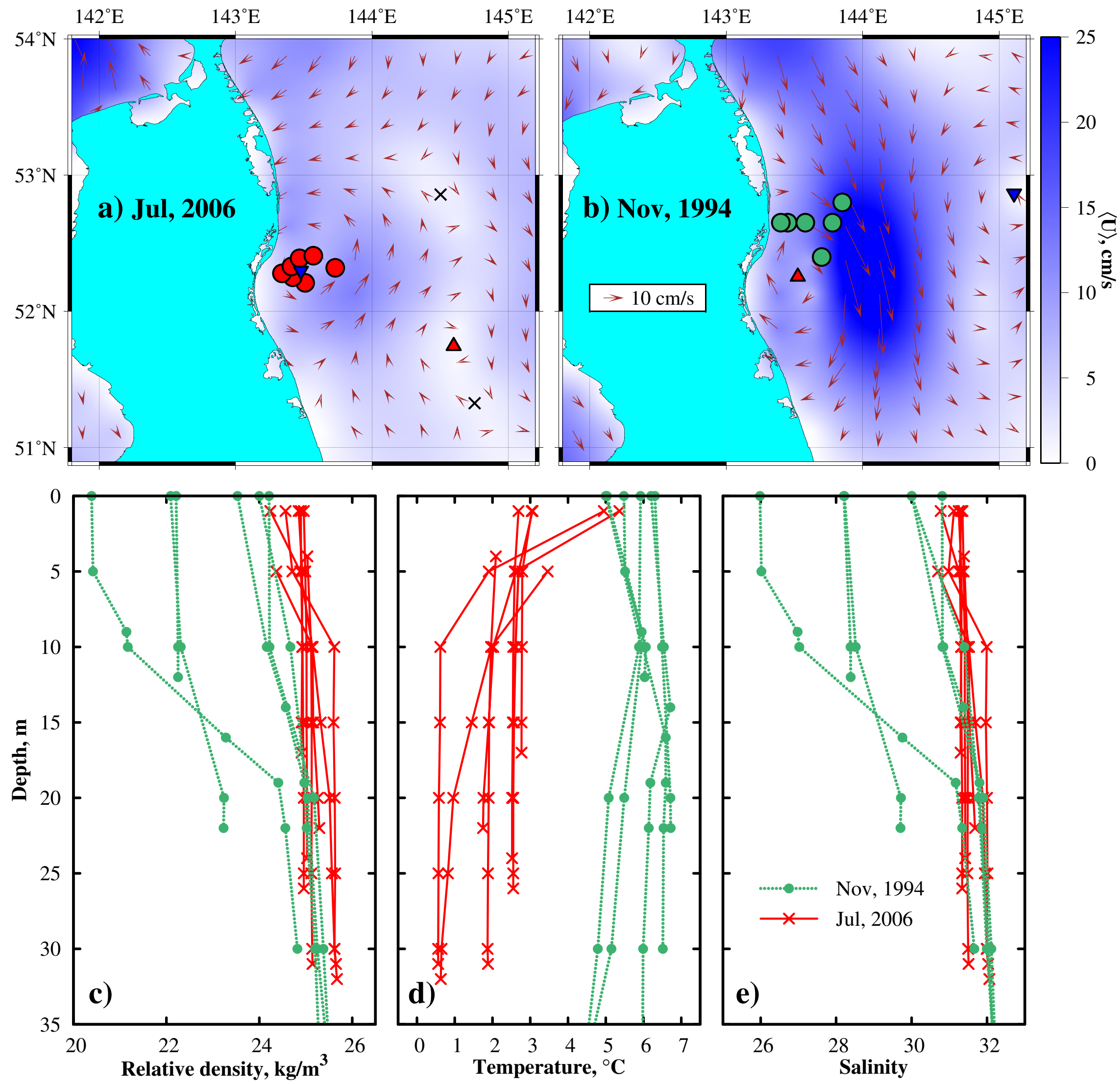

Fig. 4 The case study of the Piltun circulation cell. The altimetric AVISO velocity field averaged for **a** July 2006 and **b** November 1994 show cyclonic and anticyclonic circulations, respectively. The vertical profiles of **c** the relative density, **d** temperature, and **e** salinity obtained in the oceanographic surveys in the mesoscale cyclone area in July 2006 (*red*) and in the mesoscale anticyclone area in November 1994 (*green*). The *red and green circles* on panels **a** and **b** are the corresponding hydrocasts locations

respectively. The vertical distributions of the relative density, temperature, and salinity, collected across the Piltun cyclone in July 2006 (Fig. 4c, d and e), show that the cyclone was composed of relatively low-temperature, high-salinity, and high-density waters. These waters were originated from a subsurface layer of the OS pelagic area. The uniform vertical distributions of the temperature and salinity in the cyclone core could be an indicator of the importance of tidal mixing at the SI shelf. In the upper 10 m layer, the difference in temperature and salinity between the waters, located inside and outside of the cyclone, exceeded 3 °C and 2 pss, respectively. In November 1994, the anticyclone was composed of relatively low salinity (26–31 pss) and low density waters (20–24 kg/m^3). The salinity of surface (0–20 m) waters outside of the anticyclone (to the east) was 2–5 pss higher than that inside it.

The origin of waters, flowing along the eastern SI coast, can be tracked with the help of the Lagrangian drift maps (Prants et al. 2011; Prants et al. 2013b) which are computed backward in time as it is described in Section 2. The waters, that entered the box shown in Fig. 5a, c through its western, northern, eastern, and southern boundaries for the 3 months in the past, are shown by yellow, blue, green, and red colors, respectively. White color corresponds to the particles that had no time to reach any boundaries due to the limited time (3 months in the past) used in the inverse simulation. Most of them reached the coast, and they have been excluded from the simulation. In summer, low salinity and warm Sakhalin

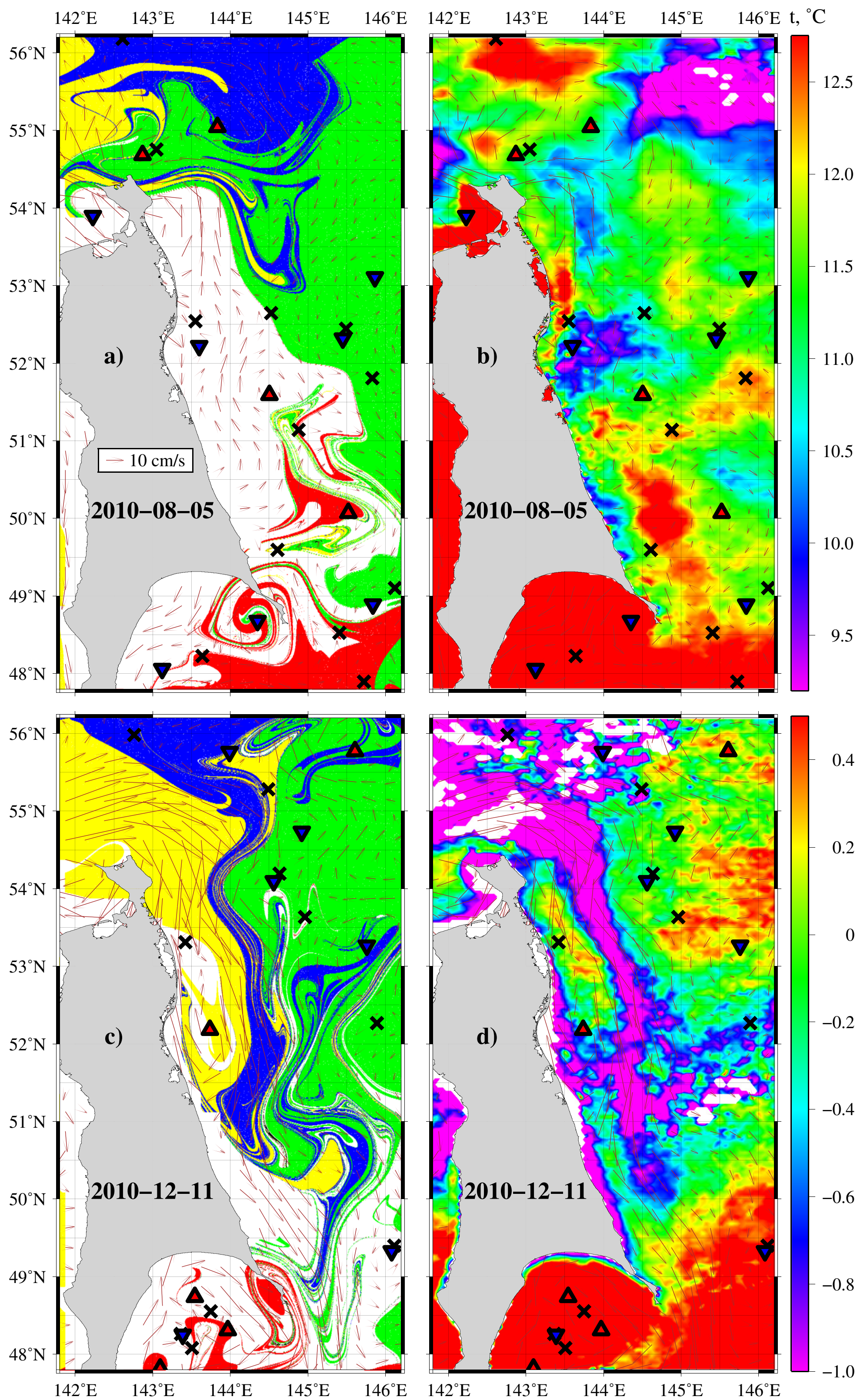

Fig. 5 **a**, **c** Lagrangian drift maps and **b**, **d** SST images (MODIS data) show examples of the seasonal variability of the flow along the eastern coast of the Sakhalin Island. **a**, **b** Formation of the cyclonic Piltun and Terpeniya mesoscale cells in summer. Intrusion of the warm "*red*" water from the southern Okhotsk Sea to the north along the Sakhalin slope is shown. **c**, **d** Formation of the anticyclonic Piltun and Terpeniya mesoscale cells in winter. Intrusion of the low-temperature "*blue*" water from the northern Okhotsk Sea to the south along the Sakhalin slope is shown. *White color* corresponds to the particles that had no time to reach any boundaries due to the limited time (3 months in the past) used in the inverse simulation. Most of them reached the coast, and they have been excluded from the simulation. SST is averaged for 3 days before and after the date indicated

Gulf waters, formed by Amur River discharge (marked by yellow), accumulate to the north of the SI (Fig. 5a). It is confirmed by the satellite SST image in Fig. 5b and distribution of the mean surface salinity in Fig. 6a. In summer, the warm "red" waters from the southern OS are advected to the north along the SI slope (Fig. 5a, b).

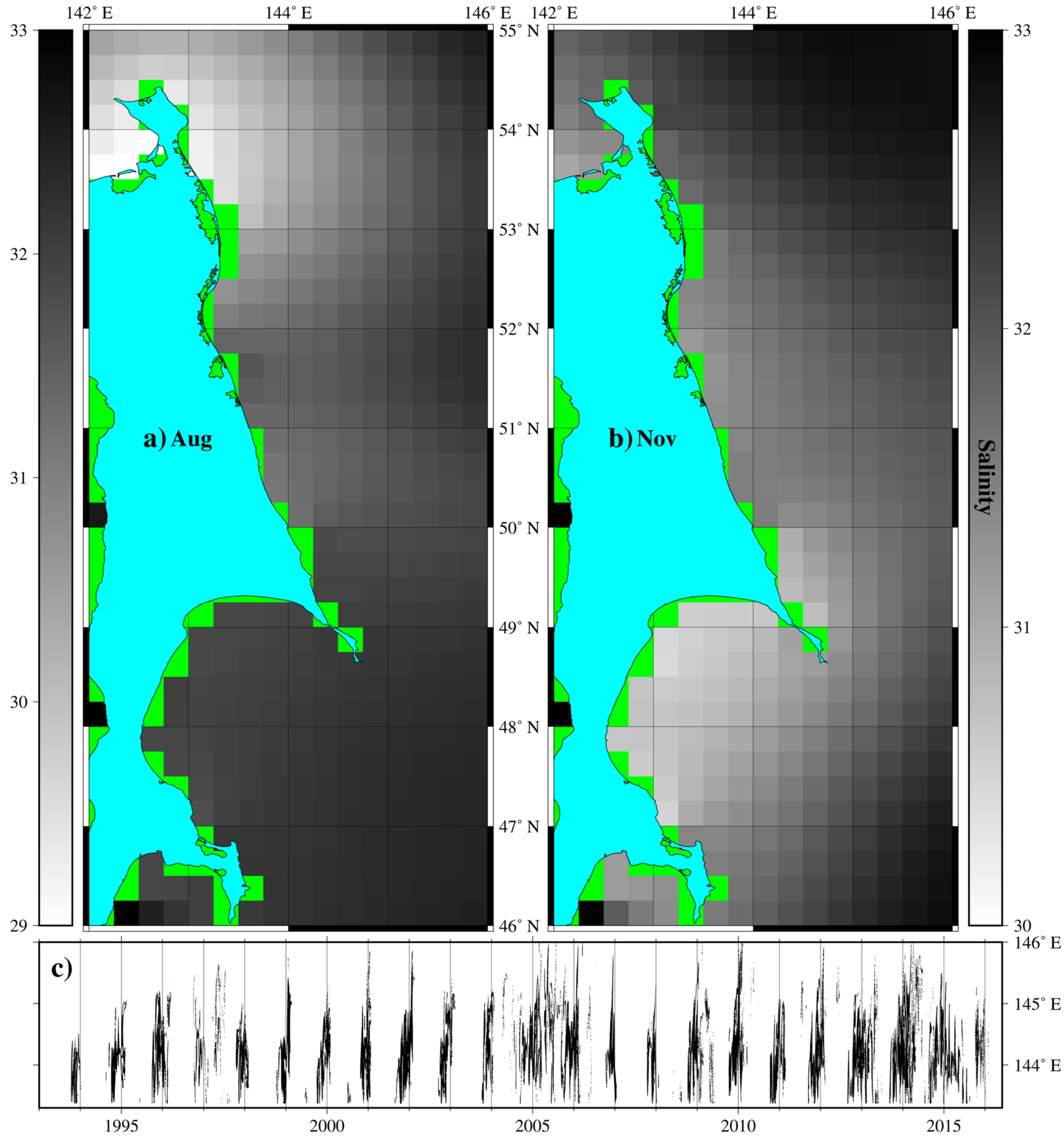

Fig. 6 Sea-surface salinity distributions averaged for **a** August and **b** November for the last 60 years (the WOD 2013 database). The values of salinity are coded by nuances of the *gray color*. Arrival of the low salinity waters (the *light gray ones*) from the Sakhalin Gulf to the Terpeniya Bay (TB in Fig. 2a) along the eastern Sakhalin shelf occurs in the cold season. **c** Simulated seasonal periodicity of the southward flow along the northeastern coast of the Sakhalin Island. It is shown when and at which longitudes the tracers launched from 1993 to 2016 at the parallel 54.25° N in the Sakhalin Gulf crossed the parallel 52.5° N off the northeastern coast of the Sakhalin Island. The *vertical straight lines* mark January, 1 for each year

The Lagrangian drift map in Fig. 5c, SST image in Fig. 5d and the mean surface salinity distribution in Fig. 6b clearly show that in late fall, less saline and relatively high temperature waters of the Sakhalin Gulf intrude southward from the northwestern shelf along the eastern SI coast. The Lagrangian map and SST imagery indicate advection of the low-temperature "blue" waters from the northern OS to the south along the SI slope in winter when the anticyclonic Piltun and Terpeniya mesoscale cells are formed.

The sea-surface salinity distributions, taken from the database WOD 2013, are shown in Fig. 6a, b with the averaging for August (panel a) and November–December (panel b) for the last 60 years. Arrival of the low salinity waters from the Sakhalin Gulf to the Terpeniya Bay (TB in Fig. 2a) along the eastern Sakhalin shelf occurs in the cold season. Seasonal variability of the flow along the eastern SI coast is illustrated in Fig. 6c. We launched 100, 000 tracers each 7 days from 1993 to 2016 along the parallel

54.25° N(139.7° E – 142.7° E), crossing the Sakhalin Gulf (SG in Fig. 1), and advected them in the AVISO velocity field. We fixed each tracer which crossed the parallel 52.5° N, the longitude of that crossing in the range from 142.5° E to 146° E and the date when it did that. The Lagrangian tracking of the Sakhalin Gulf waters clearly demonstrates seasonal periodicity of the southward flow along the eastern SI coast. Except for a couple of years, arrival of the low salinity Sakhalin Gulf waters occurred mainly in November – December at the western SI shelf (Fig. 6c).

Prevailing winds and distribution of the wind stress curl exhibit large seasonal variations in the area (Fig. 7a, b). In summer, the southerly (northward) winds along the SI are determined by the high sea level pressure center (the OS High) located over the OS. In November – December, the Aleutian Low develops in the northern Pacific, and strong northerly (southward) or northwesterly winds appear along the SI coast with a positive wind stress curl over the northern and central OS. Due to orography and wind intensification around the capes, the northward winds in summer and southward winds in fall and winter lead to the local cyclonic (June) and anticyclonic (December) wind stress curl fields along the eastern SI coast. Figure 7c, d shows temporal changes in the meridional wind and meridional velocities (daily data) at the western and eastern boundaries of the mesoscale Piltun circulation cells in July – August and November – December 2013.

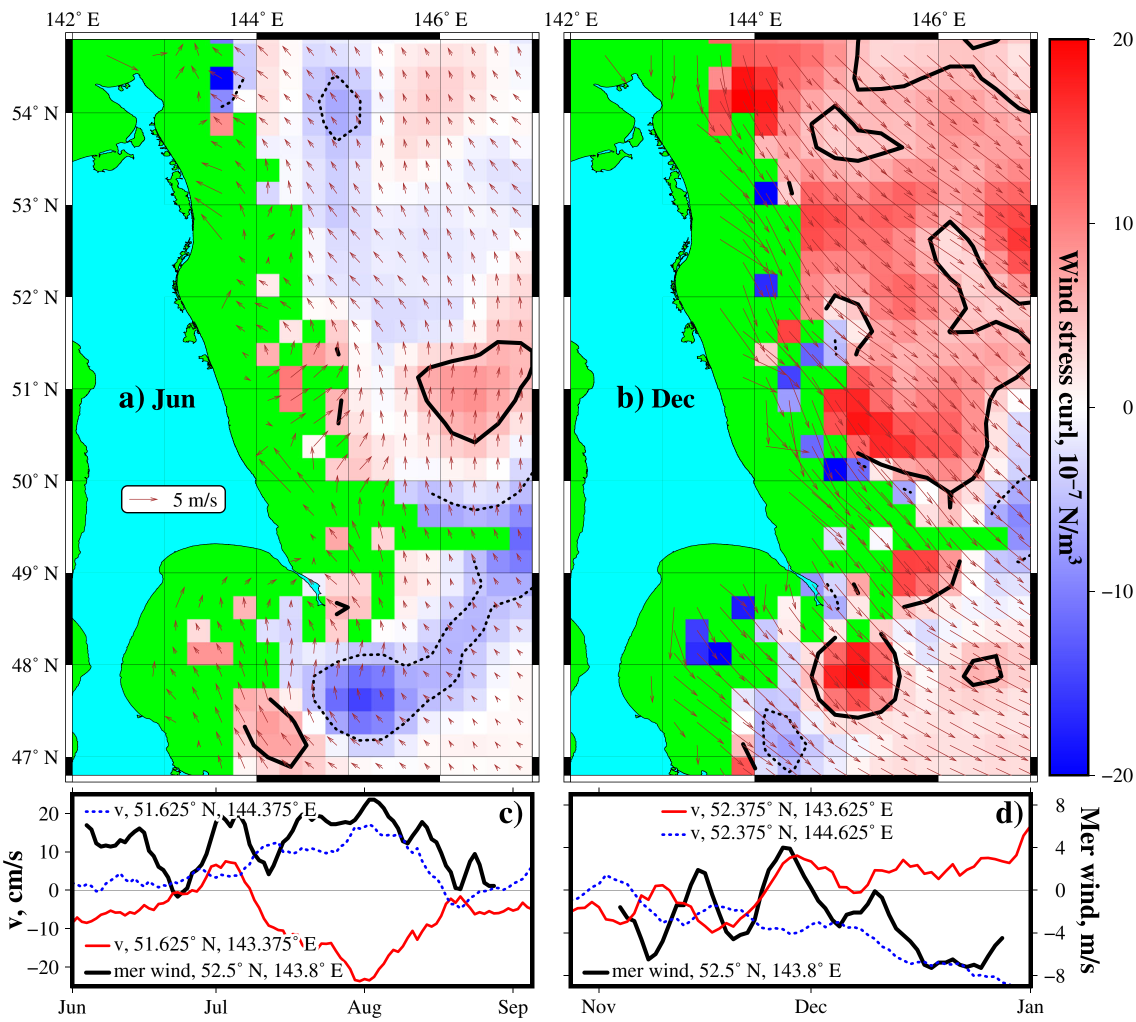

Fig. 7 The scatterometer-derived wind vectors (*the arrows*) and wind stress curl averaged for **a** June and **b** December over the period from 1999 to 2007. Values of the wind stress curl are shown by the bar in the units of 10^{-7} N m^{-3} (colored in the online version). Available data are shown by the *squares*. *Solid and dashed contour lines* show the positive (*red* in the online version) and negative (*blue* in the online version) areas of the wind stress curl, respectively. Temporal changes in the AVISO meridional velocities (v) and meridional winds (daily data) in **c** July – August and **d** November – December 2013. AVISO meridional velocities v are taken at the western (51.625° N, 143.375° E) and eastern (51.625° N, 144.375° E) boundaries of the Piltun circulation cell and shown in the units of centimeters per second by the *solid and dashed curves*, respectively. The velocity of the meridional winds is shown by the *black solid curve* in the units of meters per second

The mesoscale cyclones (anticyclones) off the SI have been observed mainly during the periods with prevailing northward (southward) winds favorable for upwelling (downwelling). At the beginning of June 2013, a weak cyclonic Piltun circulation with the meridional velocities of 0.03–0.08 m/s has been formed due to northward winds. Northward winds with the velocity of about 20 m/s during July led to generation of a mesoscale cyclone with the meridional velocities of 0.15–0.30 m/s at its boundaries. In the third decade of August after the northward winds died down, intensity of the cyclonic circulation decreased significantly. Intensification of the winter monsoon in the middle of December 2013 led to formation of the anticyclonic Piltun circulation, amplification of the north-directed currents at the shelf and south-going component of the currents along the slope.

4 Discussion

Figure 8 shows the year-to-year changes of the surface meridional velocity averaged in the area shown in Fig. 2a by the bold straight lines (48.38° N – 53.12° N, 143.38° E – 146.38° E) and the Sverdrup volume transport computed by Eq. 2 and averaged over the southern part of the OS (48° N – 54° N, 144° E – 154° E) in July and November. Because of the positive wind stress curl in November, a cyclonic circulation occurs over the northern and central OS, and the ESC flows southward along the eastern Sakhalin coast (Fig. 8b). Its surface velocity is determined by the values of the wind stress curl with the correlation coefficient $r = 0.78$. Figure 8a demonstrates that the direction and magnitude of the ESC surface velocity in July is determined by the wind stress curl over the OS with $r = 0.60$. When the wind stress curl over the OS is negative (anticyclonic) or positive (cyclonic) in July, ESC surface velocity tends to be northward or southward, respectively. We may assume that spin-up of the cyclonic gyre in the OS, forced by a positive wind stress curl over the northern part of the Sea in fall and winter, intensifies the southward transport of the ECS and causes a mesoscale anticyclonic circulation off the northeastern SI.

The wind stress curl fields from QuikSCAT show that local anticyclonic (and cyclonic) wind stress maxima along the SI coast (Fig. 7) are associated with the anticyclonic (and cyclonic) circulation cells (Figs. 2 and 3). Our results are consistent with the hypothesis of anticyclonic eddy formation due to a local anticyclonic wind stress curl associated with orography and wind intensification around the capes (Perlin et al. 2004).

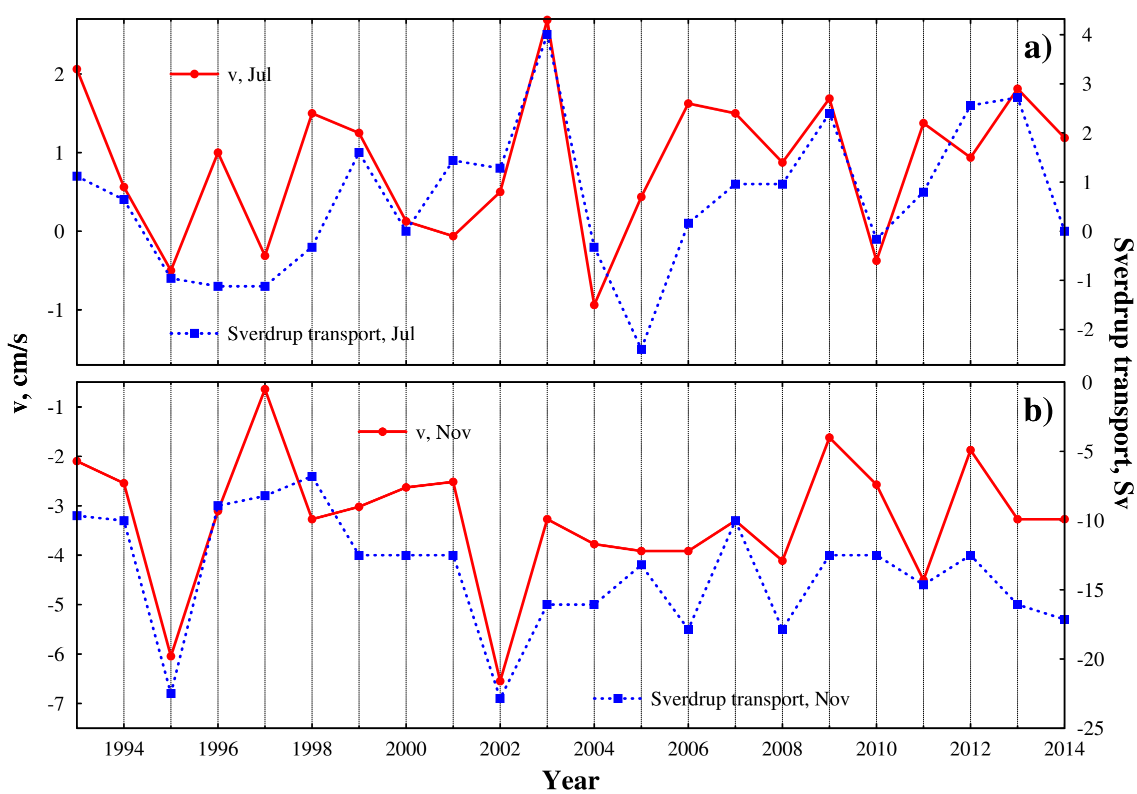

Fig. 8 (*solid lines*) Year-to-year changes in the surface meridional velocity averaged in the area 48.38° N – 53.12° N, 143.38° E – 146.38° E shown in Fig. 2a by the *bold straight lines*. (*dotted lines*) Sverdrup transport averaged over the southern Okhotsk Sea (48° N – 54° N, 144° E – 154° E)

In summer, the low salinity waters, formed by an Amur River discharge, are concentrated in the coastal area of the northern SI (Figs. 5 and 6). In fall and winter, during winter monsoon, the low salinity and low density waters are transported by the ESC from the northern end of the SI to the southern part of the OS along the eastern SI coast. Therefore, both barotropic and baroclinic effects could contribute to an intensification of the southward flow of the ESC and mesoscale anticyclone generation in fall – winter. The correlation between the meridional velocities at the boundaries of the mesoscale cyclone and the meridional wind in summer (Fig. 7a, c) could be related to the strength of the upwelling events that occur along the shelf edge of the eastern SI. The wind, directed northward along the eastern SI coast, generates an Ekman transport of water in the eastern direction toward the deep basin and hence causes an upwelling of abyssal waters (Verkhunov 1997; Rutenko et al. 2009; Rutenko and Sosnin 2014). The alongshore upwelling fronts have been often observed in satellite infrared images of the OS in summer when the presence of the seasonal thermocline provides pronounced contrasts of the SST (Fig. 5b). The upwelling in the northern and central parts of the eastern SI shelf took place from July to August. In the southern part of the region (off the Terpeniya Peninsula), an upwelling occurs during August – September. Variability of the upwelling is primarily driven by a regional wind forcing (Zhabin and Dmitrieva 2016). Decrease of the sea level and shallowing the density contours toward the shore (westward), forced by the Ekman drift, lead to the northward flow of the ESC in summer (Verkhunov 1997). The upwelling often results in formation of cyclonic eddies. The eddies can be formed by baroclinic instability of the alongshore jet (generated by the upwelling) regardless to the existence of topographic irregularities (Zhurbas et al. 2006).

The upwelling enriches the euphotic layer of the SI shelf (around 50 m) with nutrients and thereby could promote the phytoplankton bloom. Our results indicate that the extremely high biological productivity (4–6 g C m^{-2} day^{-1}) and high concentration of chlorophyll-a (3–7 μg/l), observed in July – August 1993, 1994, and 2003 (Sorokin and Sorokin 2002; Belan et al. 2005), are related to the mesoscale cyclones at the shelf edge off the northeastern SI (Piltun cyclones). The mesoscale cyclones tend to upwell nutrient-enriched deep waters into the euphotic zone thereby increasing biological community production (Falkowski et al. 1991). The extremely high concentration of chlorophyll-a, observed in the mesoscale cyclones off the northeastern SI in July – August, has been probably caused by high nutrient concentrations (NO_3 $\sim$10–20 μmol/kg, SiO_2 $\sim$15–40 μmol/kg) and low temperatures (from -2 to 1 °C) providing comfortable conditions for the large diatom phytoplankton growth.

5 Conclusions

The flow field in the ESC area is characterized by the existence of mesoscale circulation cells. Formation of the anticyclonic (November – December) and cyclonic (July – August) mesoscale circulations in this area causes seasonal flow reversals along the East Sakhalin shelf and slope. The strong seasonality in surface circulation could be explained by temporal changes in the wind stress curl and wind direction along the Sakhalin. The mesoscale cyclones generation is related to a coastal upwelling forced by northward winds and the positive wind stress curl along the Sakhalin coast. The anticyclones formation is related to inflow of low salinity waters from the Sakhalin Gulf forced by southward winds and the negative wind stress curl along the Sakhalin coast. The mesoscale cyclones and anticyclones provide water exchange between the shelf and deep basin of the OS. The mesoscale cyclonic circulation can been considered as direct and indirect causes of an increase of the biological productivity at the northeast Sakhalin shelf in summer.

Acknowledgments This work was supported by the Russian Science Foundation (project no. 16–17–10025). The altimeter products were distributed by AVISO with support from CNES.

References

Belan TA, Budaeva VD, Makarov VG, Propp LN, Selina MS, Orlova TY, Stonik IV (2005) Oceanographical and hydrobiological investigations along north east Sakhalin Island in summer 2003. Pac Oceanograph 3(1):66–69

Ebuchi N (2006) Seasonal and interannual variations in the East Sakhalin current revealed by TOPEX/POSEIDON altimeter data. J Oceanograph 62(2):171–183. doi:10.1007/s10872-006-0042-x

Falkowski PG, Ziemann D, Kolber Z, Bienfang PK (1991) Role of eddy pumping in enhancing primary production in the ocean. Nature 352(6330):55–58. doi:10.1038/352055a0

Kochergin IE, Rybalko SI, Putov VF, Shevchenko GV (1999) Hydrometeorological and ecological conditions of the Far-Eastern Seas: marine environmental impact assessment. FERHRI special issue 2, Dalnauka, Vladivostok, chap Processing of the instrumental current data collected in the Piltun-Astokh and Arkutun-Dagi oil fields, pp 96–113. [in Russian]

Kusailo OV, Shevchenko GV, Chastikov VN (2013) Extreme nonperiodic currents on the northeastern shelf of Sakhalin island. Doklady Earth Sci 448(1):97–102. doi:10.1134/s1028334x1301011x

Meier SK, Yazvenko SB, Blokhin SA, Wainwright P, Maminov MK, Yakovlev YM, Newcomer MW (2007) Distribution and abundance of western gray whales off northeastern Sakhalin Island, Russia, 2001–2003. Environ Monitor Assess 134(1–3):107–136. doi:10.1007/s10661-007-9811-2

Minervin IG, Romanyuk VA, Pishchal'nik VM, Truskov PA, Pokrashenko SA (2015) Zoning the ice cover of the Sea of Okhotsk and the Sea of Japan. Herald Russian Acad Sci 85(2):132–139. doi:10.1134/s1019331615010049

Moroshkin KV (1966) Water masses of the Okhotsk Sea. Moscow, Nauka. [in Russian]

Ohshima KI, Simizu D, Itoh M, Mizuta G, Fukamachi Y, Riser SC, Wakatsuchi M (2004) Sverdrup balance and the cyclonic gyre in the Sea of Okhotsk. J Phys Oceanograph 34(2):513–525. doi:10.1175/1520-0485(2004)034<0513:sbatcg>2.0.co;2

Perlin N, Samelson RM, Chelton DB (2004) Scatterometer and model wind and wind stress in the Oregon – Northern California coastal zone. Month Weather Rev 132(8):2110–2129. doi:10.1175/1520-0493(2004)132<2110:samwaw>2.0.co;2

Pishchalnik VM, Arhipkin VS (1999) Hydrometeorological and ecological conditions of the Far-Eastern Seas: marine environmental impact assessment. FERHRI special issue 2, Dalnauka, Vladivostok, chap Seasonal variations of the circulation on Sakhalin shelf, pp 84–95. [in Russian]

Prants SV (2013) Dynamical systems theory methods to study mixing and transport in the ocean. Physica Scripta 87(3):038,115. doi:10.1088/0031-8949

Prants SV (2014) Chaotic Lagrangian transport and mixing in the ocean. Eur Phys J Spec Topics 223(13):2723–2743. doi:10.1140/epjst/e2014-02288-5

Prants SV (2015) Backward-in-time methods to simulate large-scale transport and mixing in the ocean. Physica Scripta 90(7):074,054. doi:10.1088/0031-8949/90/7/074054

Prants SV, Uleysky MY, Budyansky MV (2011) Numerical simulation of propagation of radioactive pollution in the ocean from the Fukushima Dai-ichi nuclear power plant. Doklady Earth Sci 439(2):1179–1182. doi:10.1134/S1028334X11080277

Prants SV, Andreev AG, Budyansky MV, Uleysky MY (2013a) Impact of mesoscale eddies on surface flow between the Pacific Ocean and the Bering Sea across the Near Strait. Ocean Modell 72:143–152. doi:10.1016/j.ocemod.2013.09.003

Prants SV, Ponomarev VI, Budyansky MV, Uleysky MY, Fayman PA (2013b) Lagrangian analysis of mixing and transport of water masses in the marine bays. Izvestiya, Atmosph Ocean Phys 49(1):82–96. doi:10.1134/S0001433813010088

Prants SV, Budyansky MV, Uleysky MY (2014) Lagrangian study of surface transport in the Kuroshio Extension area based on simulation of propagation of Fukushima-derived radionuclides. Nonlin Process Geophys 21(1):279–289. doi:10.5194/npg-21-279-2014

Prants SV, Andreev AG, Budyansky MV, Uleysky MY (2015) Impact of the Alaskan Stream flow on surface water dynamics, temperature, ice extent, plankton biomass, and walleye pollock stocks in the eastern Okhotsk Sea. J Marine Syst 151:47–56. doi:10.1016/j.jmarsys.2015.07.001

Risien CM, Chelton DB (2008) A global climatology of surface wind and wind stress fields from eight years of QuikSCAT scatterometer data. J Phys Oceanograph 38(11):2379–2413. doi:10.1175/2008jpo3881.1

Rutenko AN, Sosnin VA (2014) Hydrodynamic processes on the Sakhalin shelf in the coastal Piltun area of the grey whale feeding and their correlation with atmospheric circulation. Russ Meteorol Hydrol 39(5):335–349. doi:10.3103/s1068373914050070

Rutenko AN, Khrapchenkov FF, Sosnin VA (2009) Near-shore upwelling on the Sakhalin shelf. Russ Meteorol Hydrol 34(2):93–99. doi:10.3103/s1068373909020058

Sorokin YI, Sorokin PY (2002) Microplankton and primary production in the Sea of Okhotsk in summer 1994. J Plankton Res 24(5):453–470. doi:10.1093/plankt/24.5.453

Verkhunov AV (1997) Complex studies of ecosystem of the Sea of Okhotsk, VNIRO, Moscow, chap Improvement of our knowledge about the large-scale circulation in the Okhotsk Sea, pp 6–17. Ecology of the seas of Russia, [in Russian]

Zhabin IA, Dmitrieva EV (2016) Seasonal and interannual variability of wind-driven upwelling along eastern Sakhalin Island coast based on the QuikSCAT/SeaWinds scatterometer data. Earth Res Space 2016(1–2):105–115. doi:10.7868/s0205961416010152. [in Russian]

Zhurbas V, Oh IS, Park T (2006) Formation and decay of a longshore baroclinic jet associated with transient coastal upwelling and downwelling: a numerical study with applications to the Baltic Sea. J Geophys Res Oceans 111(C4):C04,014. doi:10.1029/2005jc003079